

# ESTELA: a method for evaluating the source and travel time of the wave energy reaching a local area

Jorge Pérez · Fernando J. Méndez · Melisa Menéndez ·  
Inigo J. Losada

Received: 26 January 2014 / Accepted: 4 June 2014  
© Springer-Verlag Berlin Heidelberg 2014

**Abstract** The description of wave climate at a local scale is of paramount importance for offshore and coastal engineering applications. Conditions influencing wave characteristics at a specific location cannot, however, be fully understood by studying only local information. It is necessary to take into account the dynamics of the ocean surface over a large ‘up-stream’ wave generation area. The goal of this work is to provide a methodology to easily characterize the area of influence of any particular ocean location worldwide. Moreover, the developed method is able to characterize the wave energy and travel time in that area. The method is based on a global scale analysis using both geographically and physically based criteria. The geographic criteria rely on the assumption that deep water waves travel along great circle paths. This limits the area of influence by neglecting energy that cannot reach a target point, as its path is blocked by land. The individual spectral partitions from a global wave reanalysis are used to reconstruct the spectral information and apply the physically based criteria. The criteria are based on the selection of the fraction of energy that travels towards the target point for each analysed grid point. The method has been tested on several locations worldwide. Results provide maps that inform about the relative importance of different oceanic areas to the local wave climate at any target point. This information cannot be inferred from local parameters and agrees with information from other approaches. The

methodology may be useful in a number of applications, such as statistical downscaling, storm tracking and grid definition in numerical modelling.

**Keywords** Dynamical downscaling · Propagation · Spectrum · Statistical downscaling · Wave climate · Wave energy flux · Wave modelling

## 1 Introduction

Wave characteristics at a local scale play a major role in a wide range of issues (e.g. maritime works, navigation routes, offshore structures design, harbour operability, ecosystem distribution and flooding risk). These conditions are dominated by locally generated waves (wind sea) and waves from distant storms (swells). Hence, the need for accurate wave data has long encouraged studies on wave generation and propagation of global ocean swells. Studies by Munk (1947), Munk et al. (1963), Barber and Ursell (1948) and Snodgrass et al. (1966) contributed significantly to the scientific basis and introduced some of the currently accepted paradigms, e.g. great circle propagation and small dissipation of swells. Unfortunately, these earlier studies were limited by the availability of in situ measurements, i.e. a small number of stations concentrated in coastal areas and covering a short time period with long gaps.

More recent studies (e.g. Collard et al. 2009) take advantage of the global coverage offered by Synthetic Aperture Radar data but they face similar constraints due to the coarse spatial and temporal resolution of these data. Despite the data limitation, studies on space and time variability of wave climate have led to a huge improvement in the physics of numerical wave models. The improved physics and the availability of higher computational power have resulted in high-quality wave hindcast databases (e.g. Raschle et al. 2008; Reguero et al. 2012). The homogeneous and continuous data

---

Responsible Editor: Oyvind Breivik

This article is part of the Topical Collection on the *13th International Workshop on Wave Hindcasting and Forecasting in Banff, Alberta, Canada October 27 - November 1, 2013*

---

J. Pérez · F. J. Méndez (✉) · M. Menéndez · I. J. Losada  
Environmental Hydraulics Institute IH Cantabria, Universidad de  
Cantabria, C/Isabel Torres nº 15. Parque Científico y Tecnológico,  
39011 Santander, Spain  
e-mail: mendezf@unican.es

from wave hindcasts overcome the limitations of instrumental data being a useful tool in order to improve our understanding of wave propagation around the globe.

In this study, we propose a methodology based on hindcast data for evaluating the area of influence at any particular location and time period. Other studies have introduced different approaches to analyse characteristics of wave generation and propagation. For instance, Devaliere et al. (2009) shows a wave tracking algorithm to identify existing wave systems and Alves (2006) uses a numerical model to evaluate the contribution of swells from different ocean basins to the global wind–wave climate. Application of our method provides different information such as where the energy is generated/dissipated, how long it takes to arrive, and the variability of the area of influence between seasons or years. It is anticipated that these information can be used to aid the design of statistical or dynamical downscaling studies. Statistical downscaling methods are based on the relationship between the local wave climate and the atmospheric patterns over a region (e.g. Wang et al. 2004; Izaguirre et al. 2012; Casas-Prat et al. 2014), and dynamical downscaling is performed to focus model resolution in the desired areas (Tolman 2008). In both cases, the definition of the area of interest is a time-consuming problem, commonly solved by subjective expert criterion. This study presents a fast and objective technique to study the wave generation area that induces local wave climate.

The rest of the paper is organized as follows: Section 2 explains the methodology and is structured into four subsections: ‘geographic criteria’, ‘spectrum reconstruction’, ‘energy flux assessment’ and ‘net energy generation areas’. In Section 3, some results in the North-East Pacific, Central-East Pacific, North-West Atlantic and Indian Ocean are presented. Finally, some conclusions are given in Section 4.

## 2 Methodology

The methodology, which is henceforth referred to as ESTELA (a method for Evaluating the Source and Travel-time of the wave Energy reaching a Local Area), is intended to characterize the influence area for a specific target point. The process is summarized in a diagram in Fig. 1 and involves four sequential steps: First, geographic criteria are applied to limit the study into the relevant spatial domain. Second, the spectral reconstruction provides frequency–direction information. Third, the wave energy assessment reveals important characteristics of the wave energy that reaches the target point. Finally, the areas of gain/loss of energy are obtained.

This method requires homogeneous wave data. In this study, a global wave parameter database (Rascle et al. 2008; Rascle and Ardhuin 2012) has been used. This database was obtained by the numerical wave model WAVEWATCH III in

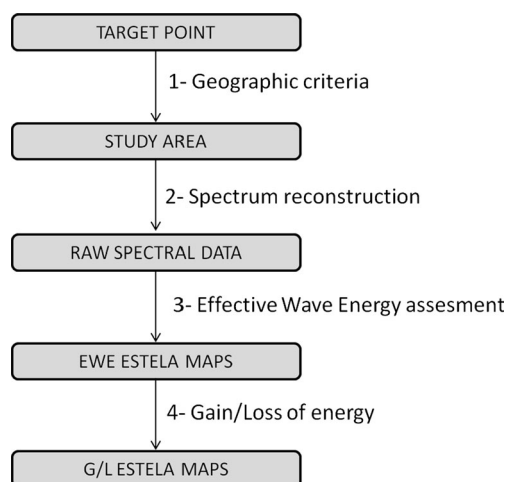


**Fig. 1** Flowchart representing the ESTELA methodology

its version 4.04 forced by winds from the Climate Forecast System Reanalysis (Saha et al. 2010). The model uses a parameterization called TEST451 (Ardhuin et al. 2010), with significant improvements for swell dissipation. The wave spectrum of the model is discretized using 24 directions and 31 frequencies and the results are provided in a spatial grid at 0.5 ° resolution and 3-h time resolution. The available catalogue from this hindcast includes parameters such as significant wave height, peak period, mean direction and directional spread for up to six partitions of the spectrum, the wind sea and five swell trains in the more general case. In this study, we use 20 years, from 1993 to 2012, of wave spectra reconstructed from these partitions.

### 2.1 Geographic criteria

The geographic criteria are applied to limit the study area by neglecting wave systems separated from the target point by land. These criteria rely on the assumption that deep water waves travel along great circle paths, which reduces the computational effort in the following steps of the methodology. This assumption has, however, several limitations due to the dynamic interaction of waves with their environment. For example, wave–current interactions are not always negligible in deep water, and processes such as refraction and diffraction may be important in shallow waters. The great circle assumption may therefore neglect contributions by energy from some cells, sited behind groups of small islands or that are partially blocked by land, to overall energy at the target point.

In order to take these limitations into account, we only neglect a source point when the area represented by that grid point is clearly blocked by land, i.e. there is a land mass that blocks all the directions in a directional sector  $\alpha \pm \Delta$ , where  $\alpha$

is the direction of the great circle between a source point and the target point and  $\Delta$  determines the width of the directional sector. We use

$$\Delta = \max\left(5, \arctan\left(\frac{dx/2 + dy/2}{r}\right)\right), \tag{1}$$

where the minimum  $\Delta$  is  $5^\circ$ ,  $dx$  and  $dy$  are the spatial resolution of the hindcast, and  $r$  is the distance between a source point and the target point.

Figure 2 shows the valid area for a target point in the North-East Atlantic Ocean. The selected area covers the whole North Atlantic basin and a section of South Atlantic Ocean, whilst the North Sea and the Caribbean Sea are not included. Note that the valid area includes all the grid points where the wave energy that reaches the target point can be generated or transformed.

### 2.2 Spectrum reconstruction

The common practice to describe a specific sea state is to use a reduced set of statistics such as the significant wave height and the mean direction. These statistics, however, do not represent the complex wave climate in some regions, where sea states are the result of several wave trains travelling in different directions. The two-dimensional wave spectrum characterizes the distribution of the wave energy among different frequencies and directions and it is considered a complete description of (phase averaged) waves on the ocean surface.

The concept of spectral partitioning introduced by Gerling (1992) allows for the identification of sub-peaks within the two-dimensional wave spectrum. The computation of the statistics of these segments represents a considerable data

reduction that preserves directional information. Consequently, these parameters have become usual output from wave models. The partitioning scheme in WAVEWATCH III is based on the method of Hanson and Phillips (2001), implemented as described in Tracy et al. (2007).

In order to reconstruct the full frequency–direction spectrum, we use four parameters obtained from spectral partitioning. Those parameters are significant wave height ( $H_s$ ), peak period ( $T_p$ ), mean direction ( $\theta$ ) and directional spread ( $\sigma$ ) for one sea and up to five swells  $\{H_{s_0}, T_{p_0}, \theta_0, \sigma_0, \dots, H_{s_5}, T_{p_5}, \theta_5, \sigma_5\}$ . Any partition can be viewed as a unimodal spectrum given by its parameters, and the multimodal spectrum can be obtained by aggregation of these unimodal spectra. We reconstruct the frequency–direction spectrum following:

$$E(f, \theta) = \sum_{i=0}^5 \rho g S_i(f) D_i(\theta), \tag{2}$$

where  $\rho$  is the water density and  $g$  is the acceleration due to gravity.  $S_i(f)$  and  $D_i(\theta)$  are the one-dimensional wave spectrum and the directional distribution for a partition  $i$ .

The one-dimensional wave spectrum  $S_i(f)$  is obtained by using a JOint North Sea WAVE Project (JONSWAP) spectrum (Hasselmann et al. 1973), where the amount of energy is determined by  $H_{s_i}$  and the distribution over the frequencies depends on  $T_{p_i}$ . We have used a JONSWAP spectrum shape with a peak enhancement parameter  $\gamma=3.3$ , since no other measures of frequency distribution were available from the wave hindcast and testing showed that this assumption has negligible effect in the assessment of the effective wave energy reaching a target point. Regarding the directional

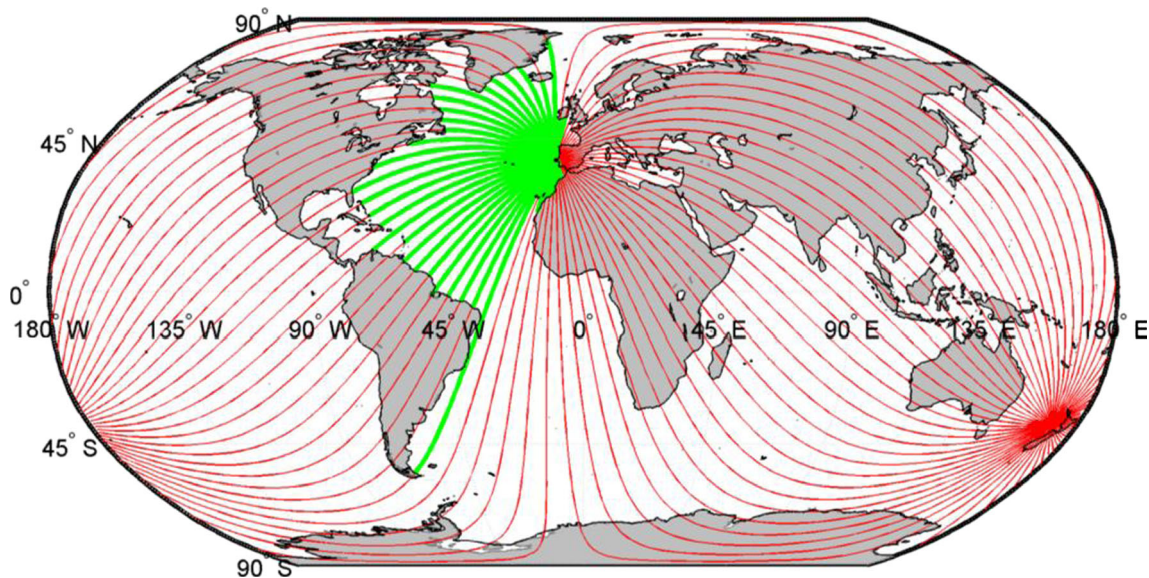


**Fig. 2** Geographic criteria for a target point P [ $10^\circ$  W,  $39^\circ$  N] in the North-East Atlantic Ocean. The selected geographic area is represented in *green* and the neglected area is represented in *red*

distribution  $D(\theta)$  we assume a cosine-type expression (e.g. Mitsuyasu et al. 1975; Holthuijsen 2007):

$$D(\theta) = A_2 \cos^{2s} \left( \frac{\theta - \alpha}{2} \right) \text{ for } -180^\circ < \theta - \alpha < 180^\circ, \quad (3)$$

where  $\theta$  is the mean direction parameter and  $\alpha$  is the direction between the source point and the target point.  $A_2$  and  $s$  are two parameters controlling the width of the distribution and depend on the directional spread parameter:

$$s = \frac{2}{\sigma^2} - 1, \quad (4)$$

$$A_2 = \Gamma(s + 1) / \left[ \Gamma\left(s + \frac{1}{2}\right) 2\sqrt{\pi} \right]. \quad (5)$$

A simple analysis to evaluate the spectrum reconstruction was performed to compare the reconstructed spectra against the original spectra from the numerical model. The evaluation in different locations and periods shows consistent results. Reconstructed spectra capture correctly the directional distribution. The frequency distribution is also represented reasonably well, although some discrepancies are found for the higher frequencies. This was expected since two parameters ( $\theta$  and  $\sigma$ ) are used to represent the directional distribution and only one parameter ( $Tp$ ) is used to represent the frequency distribution.

### 2.3 Effective energy flux assessment

The effective energy flux assessment is based on the characteristics of the spectrum and the location of the source point and the target point. Here, the effective energy flux is defined as the energy of the spectrum travelling towards the target point at the group velocity, and it is estimated to achieve the Effective Wave Energy (EWE) ESTELA maps. The effective energy is corrected by the viscous dissipation that the waves are expected to suffer during the propagation between the source and target points. In order to evaluate the relative importance of the far-field regions, the effect of other dissipation mechanisms must be taken into account. This can be assessed qualitatively by analyzing the effective energy flux in the downstream points of the great circle path.

Figure 3 shows the relevant part of the spectrum at a time  $t$  (right) for a particular great circle (left). The position of the source point with respect to the target point is defined by the distance  $r$  and the angle  $\alpha$ . The spectral density radiated towards the target point is determined by  $E_{(f;r,\alpha,t)}$ , the cross section through the spectrum  $E_{(f,\theta;r,\alpha,t)}$  at the direction  $\alpha$ . In order not to overestimate the importance of energy from distant source points, a spatial decay at a rate  $\mu$  can be

considered. A theoretical lower bound for  $\mu$  is given by the viscous theory, giving, in deep water (Dore 1978; Ardhuin et al. 2009; Collard et al. 2009)

$$\mu = 2 \frac{\rho_a}{\rho_w g c_g} \left( \frac{2\pi}{T} \right)^{5/2} \sqrt{2\nu_a}, \quad (6)$$

where  $\rho_a/\rho_w=0.0013$  is the relation between air density and water density,  $c_g = g^T/4\pi$  is the group velocity and  $\nu_a$  is the air viscosity (for a clean surface  $\nu_a=1.4 \cdot 10^{-5} \text{m}^2 \text{s}^{-1}$ ).

Viscous dissipation is responsible for a considerable loss of energy of higher frequencies. Dissipation of lower frequencies, however, is dominated by other processes. We only correct viscous dissipation because it can be considered independent of the atmospheric and oceanic conditions during the propagation. Moreover, regions where the loss of energy cannot be explained by viscous dissipation are as interesting as the regions where energy is generated.

The effective energy flux ( $F$ ) and the travel time ( $\tau$ ) at any time ( $t$ ) and position ( $r, \alpha$ ) are then:

$$F_{(r,\alpha,t)} = \int_0^\infty E_{(f;r,\alpha,t)} e^{-\mu r} c_g df, \quad (7)$$

$$\tau_{(r,\alpha,t)} = r \frac{\int_0^\infty E_{(f;r,\alpha,t)} e^{-\mu r} df}{F_{(r,\alpha,t)}}. \quad (8)$$

The effective energy flux and the travel time over a series of  $N$  sea states can be easily obtained. The effective energy flux is the sum of the valid energy fluxes divided by the number of sea states and the travel time is obtained by using the weighted mean of the group celerity:

$$\overline{F}_{(r,\alpha)} = \frac{\sum_{i=1}^N F_{(r,\alpha,t_i)}}{N}, \quad (9)$$

$$\overline{\tau}_{(r,\alpha)} = r \frac{\sum_{i=1}^N F_{(r,\alpha,t_i)} \frac{\tau_{(r,\alpha,t_i)}}{r}}{\sum_{i=1}^N F_{(r,\alpha,t_i)}}, \quad (10)$$

### 2.4 Gain/loss of energy

The effective energy flux characterizes wave propagation. In order to analyse the wave generation and dissipation, this information must be regridded to a polar grid centred at the target point. In a polar grid, the gain/loss of energy in each cell

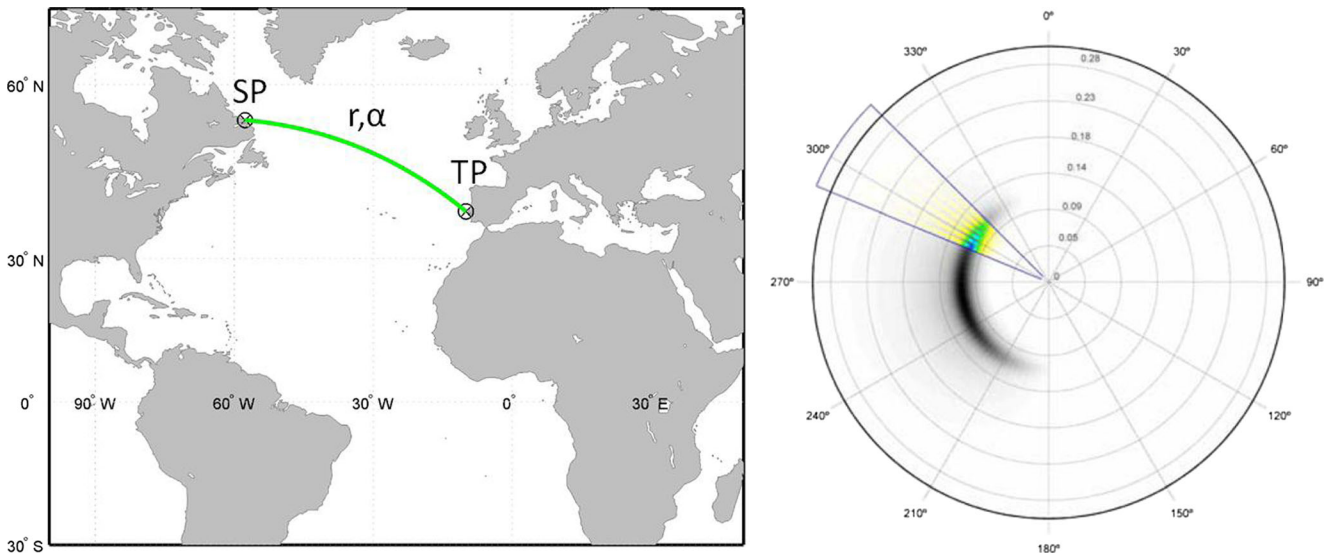


**Fig. 3** *Left* An example of the great circle between a target point near Portugal and a source-point in Canada. *Right* Wave energy spectrum at the source point. The selected cross section of wave energy that will propagate along the great circle between TP and SP is *coloured*

( $\Delta F$ ) can be viewed as the difference between the incoming and the outgoing flux along the great circle. This Lagrangian point of view, similar to the first-generation wave models, is shown in Fig. 4. Note that this approach sums the effect of the traditional wave growth and dissipation with the effect of wave components that cross the great circle.

In order to reduce the influence of the discretization,  $\overline{\Delta F}_{(r,\alpha)} = \overline{\Delta F}_{(r_{out},\alpha)} - \overline{\Delta F}_{(r_{in},\alpha)}$  is divided by the surface of the cell. The surface is the intersection between a spherical wedge and a spherical segment

$$S = S_{total} \frac{S_{wedge} S_{segment}}{S_{total} S_{total}} = 4\pi R^2 \frac{\lambda}{2\pi} \frac{|\cos(r_{in}/R) - \cos(r_{out}/R)|}{2}, \tag{11}$$

where  $R$  is the Earth radius,  $\lambda$  is the angle of the wedge and  $r_{in}$  and  $r_{out}$  are the distances between the target point and the sides of the cell. The  $\overline{\Delta F}_{(r,\alpha)}$  values are shown in the gain/loss (G/L) ESTELA map.

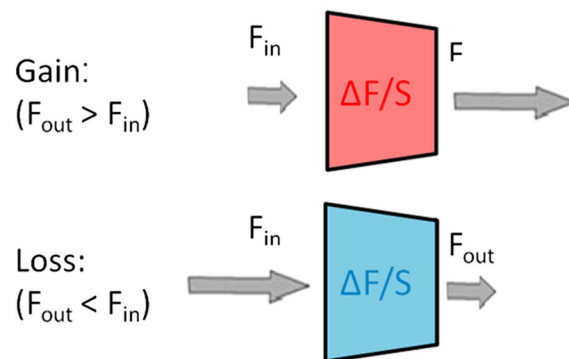
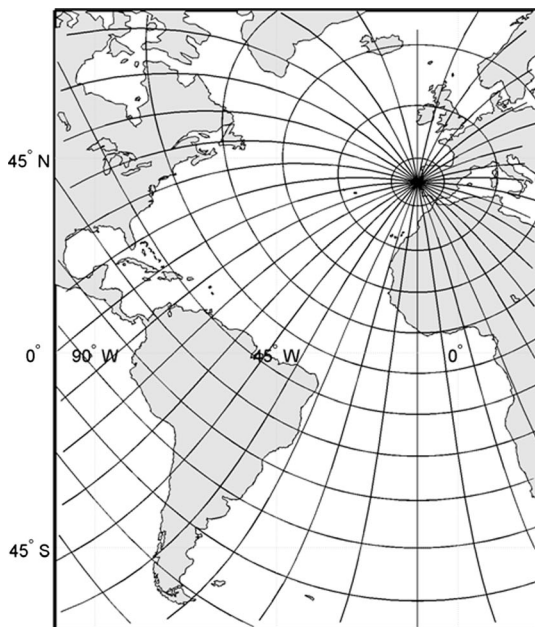


**Fig. 4** Polar grid with coarse resolution centred in a target point  $P$  [ $10^\circ$  W,  $39^\circ$  N] in the North-East Atlantic Ocean (*left*) and diagram of gain/loss of energy (*right*)

### 3 Results

In order to show the suitability of the ESTELA method at any location, four target points are selected: (i) site A [ $131^\circ$  W,  $46^\circ$  N] in the North-East Pacific, close to the Oregon state (USA); (ii) site B [ $80^\circ$  W,  $8^\circ$  S] in the Central-East Pacific, near the Peruvian coast; (iii) site C [ $10^\circ$  W,  $44^\circ$  N] in the North-East Atlantic, near the North-West Spanish coast and (iv) site D [ $55.5^\circ$  E,  $5.5^\circ$  S] in the Indian Ocean, located in the Seychelles Islands.

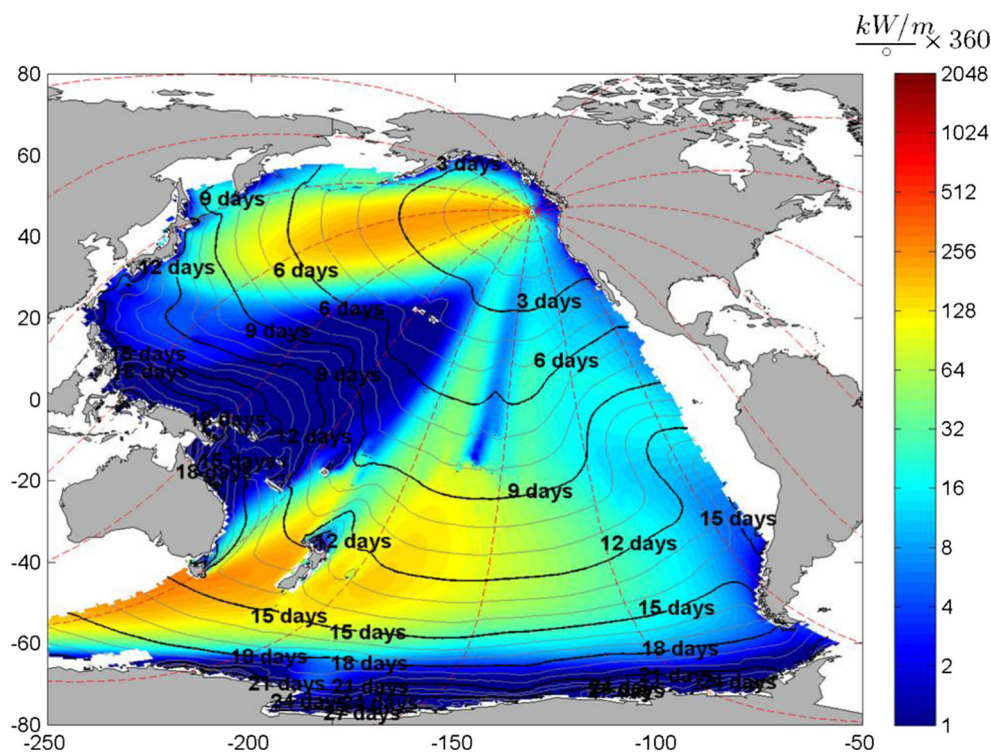
Site A is affected by the North-Pacific extra-tropical cyclone activity. Some authors have explained higher wave energy due to intensification of the Aleutian low and a strong interannual variability of wave climate related to the Pacific North America (PNA) teleconnective index (Bromirski et al. 2005; Graham and Diaz 2001). Site B is in a tropical region, affected by long-period swells that cross the entire Pacific Ocean (Young 1999) and the trade winds. Atmospheric patterns related to teleconnections between tropics, extra-tropics and high latitudes are, therefore, expected to affect the variability of the wave climate in this study site (see for instance the effect of the Southern Annular Mode (SAM), on waves in the South Hemisphere described in Hemer et al. 2010). Site C is an open location exposed to the North Atlantic extra-tropical storms. The strength and the direction of the westerly winds and storm tracks are the main climatic drivers at site C. Some authors (e.g. Woolf et al. 2002; Izaguirre et al. 2010) have found that a large fraction of the wave energy along the Atlantic European coast can be associated to the North

Atlantic oscillation (NAO). Wave climate of site D is clearly affected by tropical cyclone activity in the Indian Ocean and the penetration of swells from the Southern Ocean has been previously identified (Young 1999; Alves 2006).

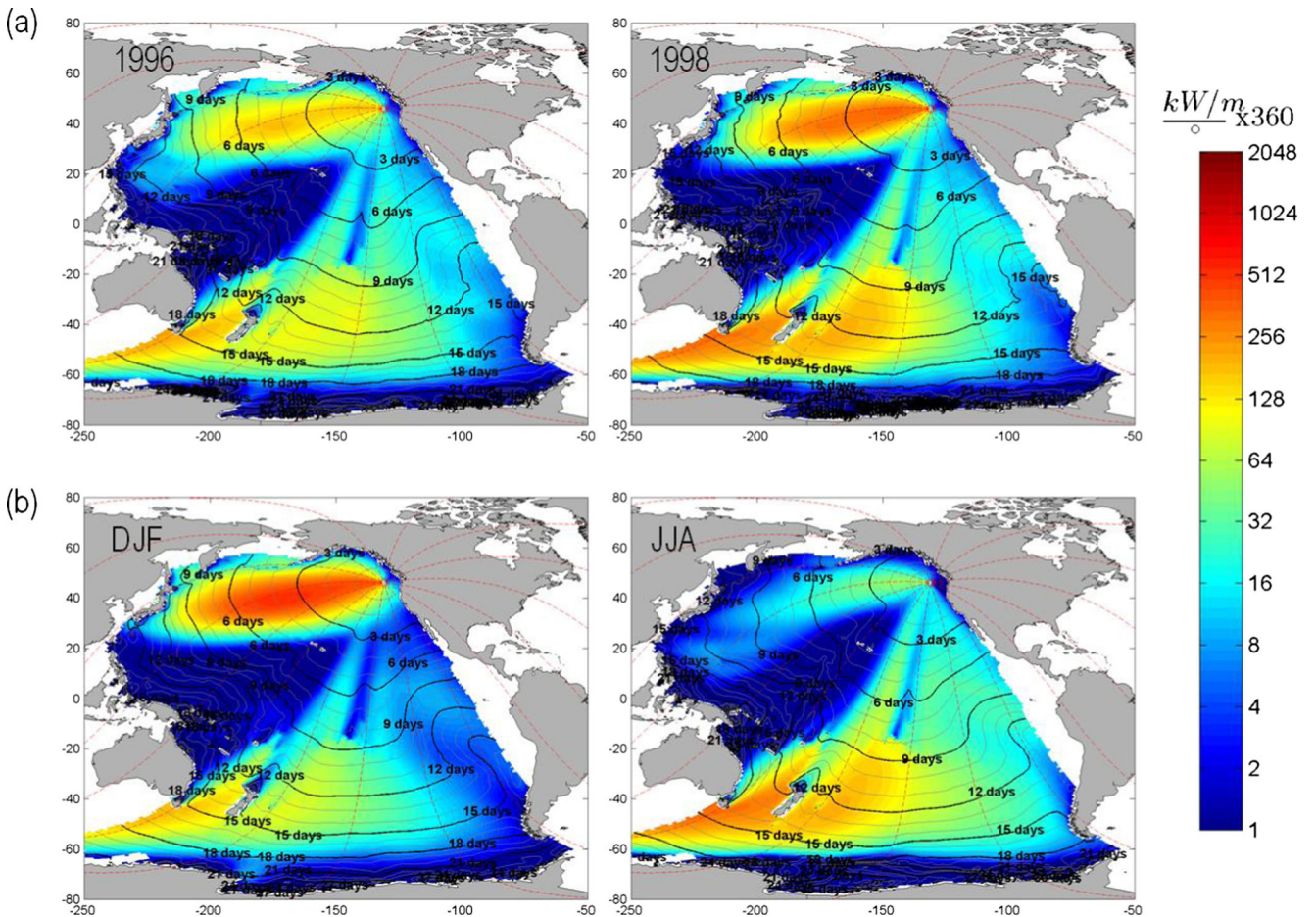
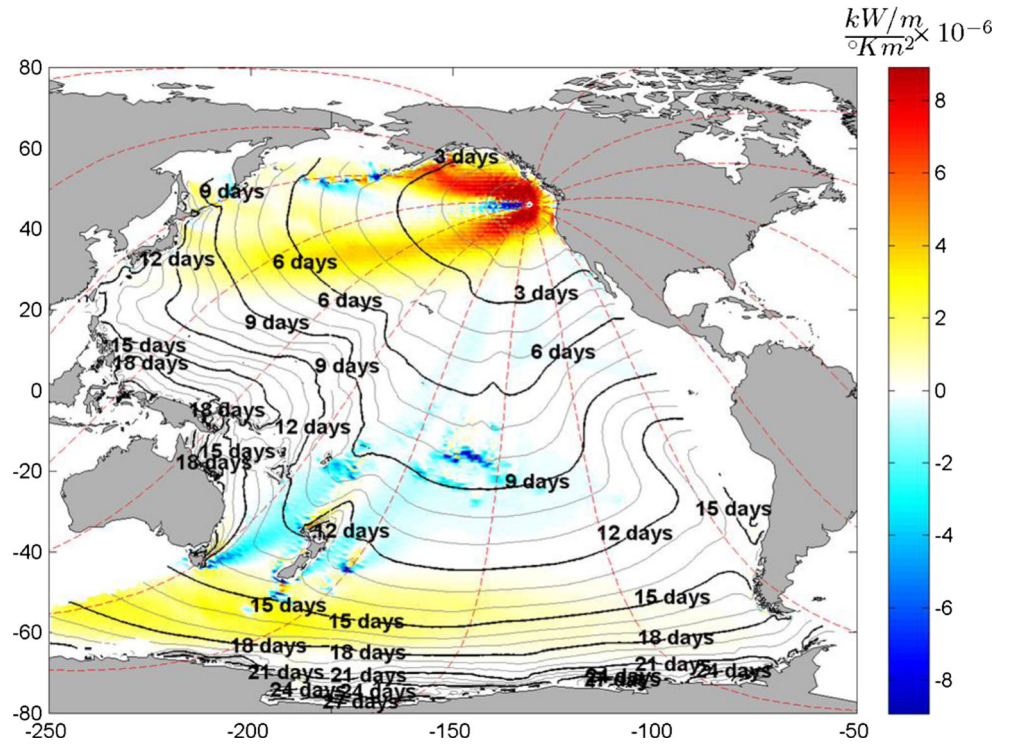
Figure 5 shows the effective mean energy flux and travel time at site A from 1993 to 2012. The coloured area shows the effective energy flux ( $\text{kW}/\text{m}/\text{degree}$ ). Red lines show the great circles of 16 directional sectors and black lines represent the travel time ( $\tau$ ) in days. Red and yellow areas represent the regions with the highest wave energy transmitted toward the target point whereas the effective energy of dark blue areas is negligible. The ESTELA map reveals two important regions: a clear energetic region eastward of the target point covering the North Pacific Ocean from  $30^\circ$  N, and a region in the Southwest Pacific near Australia and New Zealand. The second one is the source of swells travelling from SSW to reach site A during 9–14 days. Some wave energy from this region is blocked due to several Polynesian islands but the waves reaching the target point from this region should be sorted swells.

Figure 6 shows the obtained generation areas (in red) and dissipation areas (blue). In this figure, the complexity of the northern area of influence becomes more evident. There are up to 3-day swells from the north-east, up to 6-day swells from southeast and important local wind seas. Moreover, the generation and dissipation of southern swells is easily identifiable. The wave attenuation due to the small islands in French Polynesia demonstrates the importance of obstruction grids for spectral wave models as outlined in Tolman (2003) and Chawla and Tolman (2008).

**Fig. 5** Mean effective energy flux from 1993 to 2012 for site A. The coloured area is defined by the group of source points that satisfy the geographic criteria. The travel time is represented by the grey and black lines



**Fig. 6** Gain/loss of energy areas from 1993 to 2012 for site A



**Fig. 7** Mean effective energy flux in 1996 (upper left), 1998 (upper right), boreal winter (lower left) and summer (lower right) for site A

The analysis of ESTELA maps for different time periods can be used to analyse the local wave climate variability. Figure 7a shows the ESTELA map for the years 1996 (left) and 1998 (right). The spatial pattern in both years is quite similar to that of Fig. 5. The intensity of  $F$ , however, is different between the maps, with 1996 being a low-energy year whereas 1998 presents the largest values in the 20 years

analysed. Figure 7b shows the ESTELA maps during the boreal winter (December, January and February) and summer (June, July and August) seasons. These maps are quite different to each other. In winter, the northern area is clearly dominant, whilst energy from the southern hemisphere is almost negligible in the proximity of the target point. On the contrary, the energy in the northern hemisphere decreases during austral

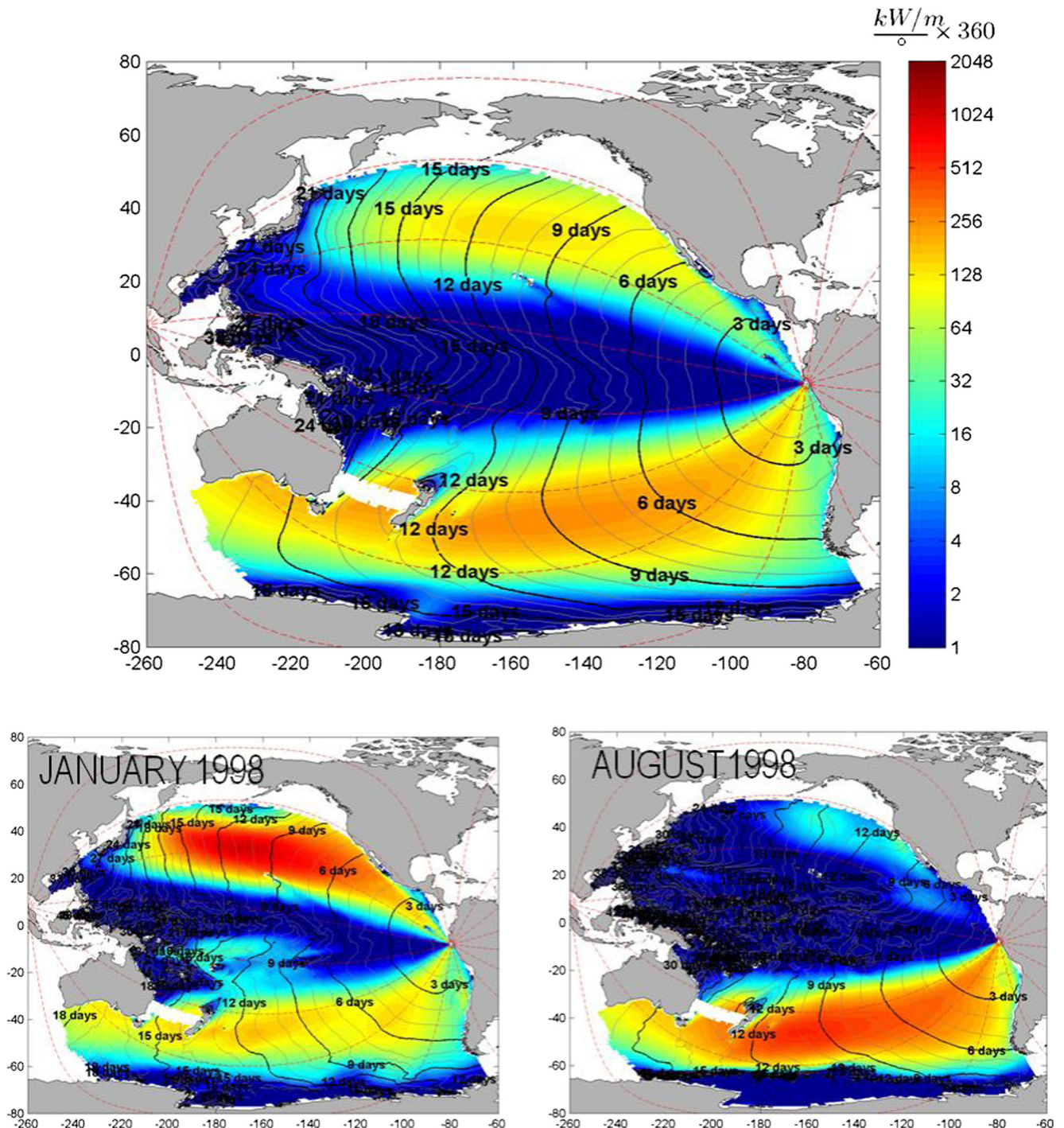


**Fig. 8** Mean effective energy flux for site B. The upper chart shows the aggregation of years from 1993 to 2012. The lower charts show January (left) and August (right) months of 1998

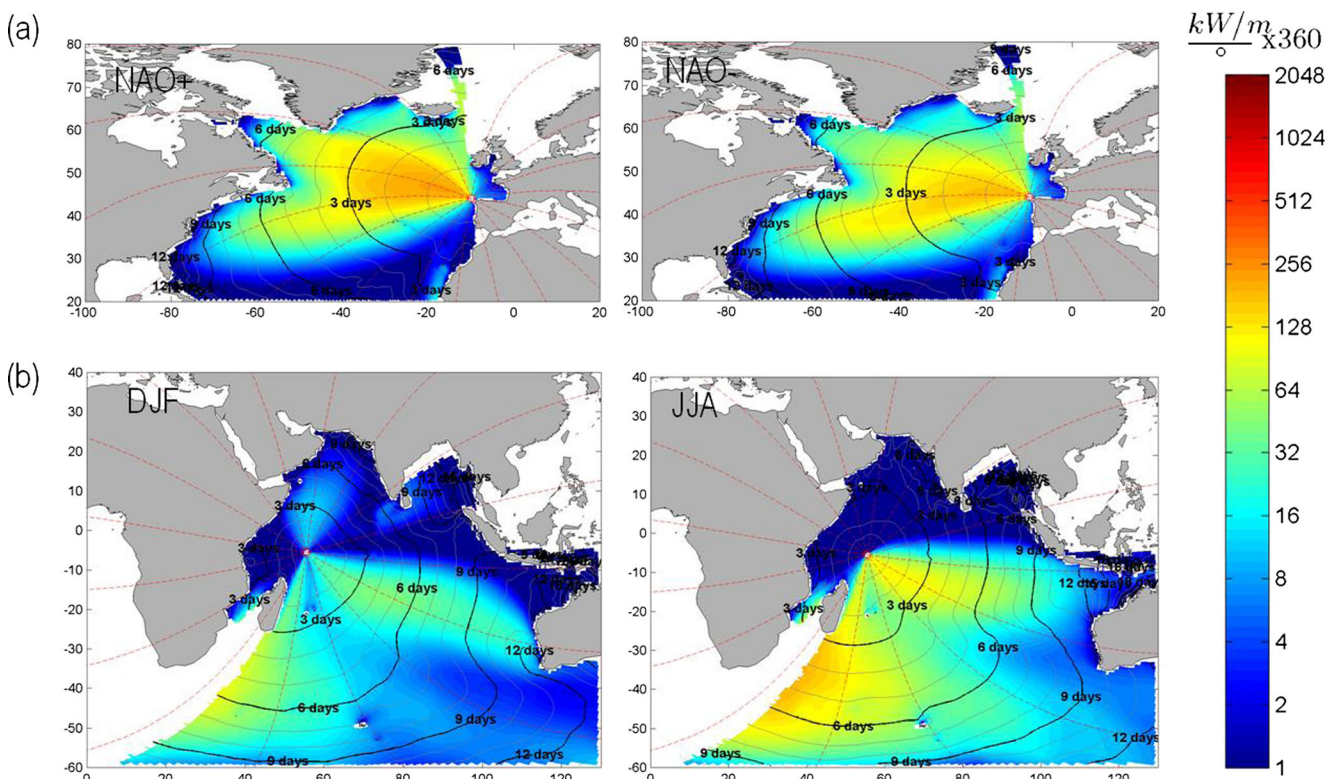
winter whereas the energy of the southern hemisphere swells increases. The ESTELA maps reveal that the interannual variability of wave climate at site A is not as large as the within a year variations.

Figure 8 shows the ESTELA maps for three different time periods at site B. The resulting ESTELA map for the 20 years (upper chart) shows an impressive spatial pattern. Two families of wave generation areas are identified: one from each hemisphere. The two areas of influence for site B show travel times of up to 2 weeks. It is interesting to note that sites A and B are affected by waves from the same extra-tropical areas of the Pacific Ocean. The effect of these waves is, however, clearly different in site B. This location is clearly exposed to the westerly winds of Southern hemisphere, which generate waves southward and southwest of site B. The wave energy in the northern hemisphere is also relevant but it is limited to a narrow directional sector between Californian Peninsula and Galapagos Islands. The lower charts of Fig. 8 show the ESTELA maps for January (left) and August (right) months of 1998, an intense El Niño year and positive SAM climate index. Swells with large energy from the northern hemisphere can reach the site B or can be non-existent depending on the month of the year.

Figure 9a shows the ESTELA maps for site C during positive and negative North Atlantic Oscillation (NAO) values. The figure shows that the effective energy in northwest

Spain is characterized by long-period swells under active storm periods (Espejo et al. 2014). The NAO pattern is one of the most prominent climate fluctuation patterns in the Northern Hemisphere (Hurrell et al. 2003). The NAO Index series obtained from the Climate Prediction Center has been used to analyse the influence of this climate index in the effective energy flux. Results show that the positive phase of NAO (NAO+) is characterized by large and long-period waves whilst the negative phase (NAO-) is characterized by smaller waves and a direction shift from northwest to west. This result agree with Izaguirre et al. (2010), which found a great influence of NAO on the extreme wave height in the North-East Atlantic, and can be related to the stronger, northward-shifted winds during NAO+ and the weaker southward-shifted winds during NAO- (Dupuis et al. 2006; Le Cozannet et al. 2011).

Figure 9b shows the ESTELA maps for site D during the boreal winter (DJF) and summer (JJA). Three families of swells are characterized: a large southwest swell generated in a region of intense winds in the Southern Ocean (more intense during austral winter); a eastern swell in the tropical Indian Ocean, a region with high occurrence of tropical cyclones, and a northern swell only appearing during boreal winter months. The ESTELA map reveals that this northern swell family can reach the tropical Indian Ocean region, in contrast with results from Alves (2006).



**Fig. 9** The upper charts show the mean effective energy flux for site C during NAO+ (left) and NAO- (right). The lower charts show the mean effective energy flux for site D during boreal winter (left) and summer (right)

## 4 Summary and conclusions

ESTELA provides an easy and objective representation of the wave climate affecting a local area based on only two parameters: the effective energy flux and the wave energy travel time. In order to obtain a good representation of directionality, these parameters are computed from the full frequency–direction spectrum. As spectral data is not always available, we propose a simple method to reconstruct the full spectrum from the statistics of spectral partitions derived from hindcast models. The reconstructed spectra show a good agreement with direct output spectra and may be useful for a range of applications.

The computational effort of ESTELA is very low because it is based on precomputed hindcast data. We would like to highlight, nevertheless, that the ESTELA results depend on the quality of the forcings and the physics scheme used in the wave model. In order to evaluate the importance of these choices, the results were compared with previous results (not shown) based on a different hindcast forced by NCEP-NCAR reanalysis and using Tolman and Chalikov (1996) source terms. As expected, some differences in magnitude were found, the spatial patterns, however, were qualitatively similar.

The results in the analysed locations offer a new tool for understanding regions of wave generation and the extent of swell propagation over the global ocean. For instance, the maps show the effects of model representation of small islands on the wave climate at distant locations and the time variability of wave generation areas. In this paper, we have analysed climatologies and seasonal and interannual variability but ESTELA can be used for a range of applications and in different time scales, from hours (footprints of extreme storms) to long term (climate change impact in the swell generation areas). For instance, Camus et al. (2014) uses ESTELA maps information to characterize the footprint of the wave climate and to automate the definition of the predictor spatial domain corresponding to the swell wave component.

**Acknowledgments** The work was partly funded by the project iMar21 (CTM2010-15009) from the Spanish Government and the FP7 European project CoCoNet (287844). The authors would also like to acknowledge the valuable suggestions made by Paula Camus, Antonio Espejo and Antonio Tomas. We also thank the anonymous reviewers for their comments and suggestions.

## References

- Alves J-HGM (2006) Numerical modeling of ocean swell contributions to the global wind–wave climate. *Ocean Model* 11(1–2):98–122. doi:10.1016/j.ocemod.2004.11.007
- Ardhuin F, Chapron B, Collard F (2009) Observation of swell dissipation across oceans. *Geophys Res Lett* 36, L06607. doi:10.1029/2008GL037030
- Ardhuin F, Rogers E, Babanin AV, Filipot J-F, Magne R, Roland A et al (2010) Semiempirical dissipation source functions for ocean waves. Part I: definition, calibration, and validation. *J Phys Oceanogr* 40(9):1917–1941. doi:10.1175/2010JPO4324.1
- Barber NF, Ursell F (1948) The generation and propagation of ocean waves and swell. I. Wave periods and velocities. *Philos Trans R Soc Lond* 240A:527–560
- Bromirski PD, Cayan DR, Flick RE (2005) *J Geophys Res* 110, C03005. doi:10.1029/2004JC002398
- Camus P, Méndez FJ, Losada IJ, Menéndez M, Espejo A, Pérez A, Rueda A, Guanche Y (2014) A method for finding the optimal predictor indices for local wave climate conditions. This issue
- Casas-Prat M, Wang XL, Sierra JP (2014) A physical-based statistical method for modeling ocean wave heights. *Ocean Model* 73:59–75
- Chawla A, Tolman HL (2008) Obstruction grids for spectral wave models. *Ocean Model* 22(1–2):12–25. doi:10.1016/j.ocemod.2008.01.003
- Collard F, Ardhuin F, Chapron B (2009) Monitoring and analysis of ocean swell fields from space: new methods for routine observations. *J Geophys Res* 114(C7), C07023. doi:10.1029/2008JC005215
- Devaliere E-M, Hanson JL, Luettich R (2009) Spatial tracking of numerical wave model output using a spiral search algorithm. 2009 WRI World Congress on Computer Science and Information Engineering, 404–408. doi:10.1109/CSIE.2009.1021
- Dore BD (1978) Some effects of the air–water interface on gravity waves. *Geophys Astrophys Fluid Dyn* 10:215–230
- Dupuis H, Michel D, Sottolichio A (2006) Wave climate evolution in the Bay of Biscay over two decades. *J Mar Syst* 63(3–4):105–114. doi:10.1016/j.jmarsys.2006.05.009
- Espejo A, Camus P, Losada IJ, Méndez FJ (2014) Spectral ocean wave climate variability based on atmospheric circulation patterns. *J Phys Oceanogr*. doi:10.1175/JPOD-13-0276.1
- Gerling TW (1992) Partitioning sequences and arrays of directional ocean wave spectra into component wave systems. *J Atmos Ocean Technol* 9(4):444–458. doi:10.1175/1520-0426(1992)009<0444:PSAAOD>2.CO;2
- Graham NE, Diaz HF (2001) Evidence for intensification of North Pacific winter cyclones since 1948. *Bull Am Meteorol Soc* 82:1869–1893
- Hanson JL, Phillips OM (2001) Automated analysis of ocean surface directional wave spectra. *J Atmos Ocean Technol* 18:177–293
- Hasselmann K et al (1973) Measurements of wind–wave growth and swell decay during the Joint North Sea Wave Project. *Ergänzungsheft zur Deutschen Hydrographischen Zeitschrift Reihe* 8(12):1–95, suppl. A
- Hemer MA, Church JA, Hunter JR (2010) Variability and trends in the directional wave climate of the Southern Hemisphere. *Int J Climatol* 30:475–491
- Holthuijsen LH (2007) *Waves in oceanic and coastal waters*. Cambridge University Press, Cambridge, p 387
- Hurrell JW, Kushnir Y, Ottersen G, Visbeck M (2003) An overview of the North Atlantic oscillation. *Geophys Monogr-Am Geophys Union* 134:1–36
- Izaguirre C, Méndez FJ, Menéndez M, Luceño A, Losada IJ (2010) Extreme wave climate variability in southern Europe using satellite data. *J Geophys Res*, 115, C04009 J
- Izaguirre C, Menéndez M, Camus P, Mendez FJ, Minguez R, Losada IJ (2012) Exploring the interannual variability of extreme wave climate in the Northeast Atlantic Ocean. *Ocean Model* 59–60:31–40
- Le Cozannet G, Lecacheux S, Delvallee E, Desramaut N, Oliveros C, Pedreros R (2011) Teleconnection Pattern influence on sea–wave climate in the Bay of Biscay. *J Clim* 24(3):641–652. doi:10.1175/2010JCLI3589.1
- Mitsuyasu H, Tsai F, Suhara T, Mizuno S, Ohkusu M, Honda T, Rikiishi K (1975) Observations of the directional spectrum of ocean waves using a cloverleaf buoy. *J Phys Oceanogr* 5(4):750–760

- Munk W (1947) Tracking storms by forerunners of swell. *J Meteorol* 4(2): 45–57
- Munk WH, Miller GR, Snodgrass FE, Barber NF (1963) Directional recording of swell from distant storms. *Philos Trans R Soc A Math Phys Eng Sci* 255(1062):505–584. doi:[10.1098/rsta.1963.0011](https://doi.org/10.1098/rsta.1963.0011)
- Raschle N, Ardhuin F (2012) A global wave parameter database for geophysical applications. Part 2: Model validation with improved source term parameterization. *Ocean Model*. doi:[10.1016/j.ocemod.2012.12.001](https://doi.org/10.1016/j.ocemod.2012.12.001)
- Raschle N, Ardhuin F, Queffelec P, Croizé-Fillon D (2008) A global wave parameter database for geophysical applications. Part 1: Wave–current–turbulence interaction parameters for the open ocean based on traditional parameterizations. *Ocean Model* 25(3–4):154–171. doi:[10.1016/j.ocemod.2008.07.006](https://doi.org/10.1016/j.ocemod.2008.07.006)
- Reguero BG, Menéndez M, Méndez FJ, Mínguez R, Losada IJ (2012) A Global Ocean Wave (GOW) calibrated reanalysis from 1948 onwards. *Coast Eng* 65:38–55. doi:[10.1016/j.coastaleng.2012.03.003](https://doi.org/10.1016/j.coastaleng.2012.03.003)
- Saha S, Moorthi S, Pan H-L, Wu X, Wang J, Nadiga S et al (2010) The NCEP climate forecast system reanalysis. *Bull Am Meteorol Soc* 91(8):1015–1057. doi:[10.1175/2010BAMS3001.1](https://doi.org/10.1175/2010BAMS3001.1)
- Snodgrass FE, Groves GW, Hasselmann KF, Miller GR, Munk WH, Powers WH (1966) Propagation of ocean swell across the Pacific. *Philos Trans R Soc A Math Phys Eng Sci* 259(1103):431–497. doi:[10.1098/rsta.1966.0022](https://doi.org/10.1098/rsta.1966.0022)
- Tolman HL (2003) Treatment of unresolved islands and ice in wind wave models. *Ocean Model* 5(3):219–231. doi:[10.1016/S1463-5003\(02\)00040-9](https://doi.org/10.1016/S1463-5003(02)00040-9)
- Tolman HL (2008) A mosaic approach to wind wave modeling. *Ocean Model* 25(1–2):35–47. doi:[10.1016/j.ocemod.2008.06.005](https://doi.org/10.1016/j.ocemod.2008.06.005)
- Tolman HL, Chalikov D (1996) Source terms in a third-generation wind-wave model. *J. Phys. Oceanogr*, 26, 2497–2518
- Tracy B, Devaliere E-M, Nicolini T, Tolman HL, Hanson JL (2007) Wind sea and swell delineation for numerical wave modeling. In 10th international workshop on wave hindcasting and forecasting & coastal hazards symposium, JCOMM Tech. Rep. 41, WMO/TD-No. 1442. Paper P12
- Wang XL, Zwiers FW, Swail VR (2004) North Atlantic Ocean wave climate change scenarios for the twenty-first century. *J Clim* 17: 2368–2383
- Woolf DK, Challenor PG, Cotton PD (2002) Variability and predictability of the North Atlantic wave climate. *J Geophys Res C: Oceans* 107(10):3145 doi:[10.1029/2001JC001124](https://doi.org/10.1029/2001JC001124)
- Young IR (1999) Seasonal variability of the global ocean wind and wave climate. *Int J Climatol* 19:931–950